NANO · MICRO small
www.small-journal.com

Effect of the Photoexcitation Wavelength and Polarization on the Generated Heat by a Nd-Doped Microspinner at the Microscale

*Elisa Ortiz-Rivero, Carlos D. González-Gómez, Raúl A. Rica, and Patricia Haro-González**

Thermal control at small scales is critical for studying temperature-dependent biological systems and microfluidic processes. Concerning this, optical trapping provides a contactless method to remotely study microsized heating sources. This work introduces a birefringent luminescent microparticle of $NaLuF_4$:Nd^{3+} as a local heater in a liquid system. When optically trapped with a circularly polarized laser beam, the microparticle rotates and heating is induced through multiphonon relaxation of the Nd^{3+} ions. The temperature increment in the surrounding medium is investigated, reaching a maximum heating of ≈5 °C within a 30 µm radius around the static particle under 51 mW laser excitation at 790 nm. Surprisingly, this study reveals that the particle's rotation minimally affects the temperature distribution, contrary to the intuitive expectation of liquid stirring. The influence of the microparticle rotation on the reduction of heating transfer is analyzed. Numerical simulations confirm that the thermal distribution remains consistent regardless of spinning. Instead, the orientation-dependence of the luminescence process emerges as a key factor responsible for the reduction in heating. The anisotropy in particle absorption and the lag between the orientation of the particle and the laser polarization angle contribute to this effect. Therefore, caution must be exercised when employing spinning polarization-dependent luminescent particles for microscale thermal analysis using rotation dynamics.

1. Introduction

Temperature is one of the most important parameters in life sciences, playing a critical role in many physical, biological, and chemical processes. Its control is essential in thermal treatments at the microscale, understood as the procedures of driving a part of the body or a system above its normal temperature in a controlled way for a defined period. They are relevant for a myriad of experiments such as polymerase chain reaction,[1] digital microfluidics,[2] protein crystallization,[3] mixing,[4] hyperthermia, or diathermia treatments (i.e., driving selectively malignant cells and tissues up to the cytotoxic level).[5] Up to now, the increase in temperature in such experiments has been achieved after the massive incorporation of heaters into the system, which presents the drawback of being an uncontrollable method. Nevertheless, in multiple of these applications, the integration of the heating source into the studied system requires to avoid excessive heating that could create undesirable damage in its surroundings. In this sense, micro- and nanoparticles appear as real alternatives to carry out selective, accurate, and efficient thermal treatments in microfluidics.[6] In particular, the recent development of particles capable of efficient heat generation under laser excitation has attracted much interest in the last few years.[7] Particles whose size and appropriate coating or surface functionalization allow them to be specifically recognized by the cell for single-cell analysis are particularly appealing.[8]

For an efficient thermal performance and better understating of the process, apart from selecting the appropriate heating

E. Ortiz-Rivero, P. Haro-González
Nanomaterials for Bioimaging Group
Departamento de Física de Materiales
Facultad de Ciencias & Instituto de materiales Nicolás Cabrera
Universidad Autónoma de Madrid
Madrid 28049, Spain
E-mail: patricia.haro@uam.es

C. D. González-Gómez, R. A. Rica
Nanoparticles Trapping Laboratory
Department of Applied Physics
Universidad de Granada
Granada 18071, Spain

C. D. González-Gómez
Department of Applied Physics II
Universidad de Málaga
Málaga 29071, Spain

R. A. Rica
Research Unit "Modeling Nature" (MNat)
Universidad de Granada
Granada 18071, Spain

DOI: 10.1002/smll.202308534

method, it is necessary to monitor the heating mechanism.[7b,9] In this work, temperature monitoring of thermal effects at the microscale is carried out by the so-called luminescent thermometers,[10] a popular method that has been widely discussed in the field of nanothermometry.[11]

In addition, to achieve full control of the heating process, a contactless manipulation technique is required since it can make possible the remote manipulation of heaters at the micro- and nanoscale, providing full control during the thermal treatment. One of these techniques is optical trapping (OT), which has emerged as a reliable method for achieving remote and precise translation and rotational control over micro- and nanostructures.[12] OT is based on the optical forces and torques exerted by a tightly focused laser beam on a single micro- or nanoparticle due to a momentum exchange or to the field-induced changes in their polarizability, respectively.[13] The type of the optically trapped particle (composition, doping ions, concentration, etc.) can determine its functionality. For example, if the particle is doped with lanthanide ions, its luminescence can be excited by using a trapping laser with an appropriate wavelength. Then, the luminescence mechanisms of a single particle can be studied and exploited for different applications. In particular, particles doped with a high content of Nd^{3+} ions are demonstrated to induce local heating in their surroundings due to multiphonon relaxation from the excited states of the Nd^{3+} ions or by emission quenching mediated by closely located non-radiative centers.[9,14] Their performance as heating particles can be determined by the thermal loading or temperature rate, c, which is defined as the temperature increment per unit of power generated by the particle, following the expression:

$$T\ (P) = T_0\ + cP \tag{1}$$

where T_0 is the initial temperature at room conditions and P is the applied power of the trapping laser.

In this sense, Bednarkiewicz et al. were the first to demonstrate the ability of Nd^{3+}-doped nanoparticles as nanoheaters, reporting a temperature rate of 0.8 °C mW^{-1}.[7c] Thus, a trapped Nd^{3+}-doped microparticle has a high potential as a local heater.

In addition, as light carries not only linear momentum but can also carry spin angular momentum if the beam is circularly polarized, the rotation of a trapped particle can be achieved by the induced optical torque.[15] In general, the induced torque from the transport of the incident waves is conservative and transient, whereas the torque due to the transport of angular momentum is non-conservative and can continuously rotate particles through their absorption, birefringence, or asymmetry.[16] For a disk-shaped crystalline microparticle, which is a positive uniaxial birefringent crystal, its optical axis is perpendicular to the two basal facets of the crystals. When optically trapped by a single Gaussian laser beam, an optical torque will be generated due to the non-spherical and birefringent nature of the trapped microdisk, and torque equilibrium will determine its orientation within the optical trap. In this case, the stable orientation is achieved when the microdisk is orientated in its vertical position and its optical axis is parallel to the electric field vector of the laser trapping beam.[17] The optical torque applied to the birefringent microdisk is as follows:

$$\tau_{opt} = \frac{\Delta\sigma P}{\omega} \tag{2}$$

where $\Delta\sigma$ is the change in polarization, P is the laser power, and ω the angular frequency of the laser beam.

If the trapping beam is circularly polarized, the birefringent disk-shaped microparticle acts as a waveplate that changes the polarization state of the incident light, which results in a variation of the angular momentum and the appearance of a hydrodynamic rotational drag that hinders the rotation. When the hydrodynamic drag balances the optical torque, the particle reaches a terminal angular velocity, given by the rotational Stokes drag torque:[18]

$$\tau_{drag} = \frac{32}{3}\ \mu R^3 \tag{3}$$

where μ is the viscosity of the medium, R the radius of the microdisk, and $\Omega = 2\pi f$ its angular frequency with f the rotation rate. By equating, $\tau_{drag} = \tau_{opt}$, the angular frequency of a hexagonal birefringent microdisk is given by:

$$\Omega\ = \left(\frac{3}{32}\right)\ \left(\frac{\Delta\sigma P}{\omega\mu R^3}\right) = \alpha\frac{P}{\mu\,(T)} \tag{4}$$

where, $\alpha\ = (\frac{3}{32})\ (\frac{\Delta\sigma}{\omega R^3})$, is a constant that depends on the characteristics of light and the morphology of the particle.

Equation (4) shows that the rotational rate of the microdisk, Ω, depends linearly on the optical power, P. In addition, it is affected by temperature through the viscosity of the medium, $\mu\ = \mu(T)$.[19] Thus, if there is heating, the microdisk will increase its rotational rate due to the viscosity decrease with temperature. For steady-state creeping flow, in an infinite viscous medium, driven by a rotating particle, the fluid flow at any radius can be characterized by an angular velocity.[20] The technological implications of this phenomenon are tremendous; a miniature rotating device can be a powerful instrument to measure properties of microscopic bio-systems.[21] For example, they have been demonstrated to be capable of measuring microscopic viscosity,[22] studying and manipulating cells[23] or to determine the torsional elasticity of single molecules.[24] Their rotation rate can be as high as hundreds of Hz, as in calcite and vaterite microcrystals in fluids.[25] The rotation speed record in an aqueous solution is held by a trapped gold nanorod, reaching up to 42 kHz (2.5 million revolutions per minute).[26] Consequently, if a luminescent microparticle presents these features, it can be implemented as a remotely controlled microheater and microrotor capable of increasing the temperature and, at the same time, stirring its surrounding fluid. As a result, it can provide a full control during thermal treatments or mixture processes in the microscale.

For this application, neodymium-doped particles based on birefringent inorganic crystalline host matrixes are ideal candidates, particularly fluoride host lattices due to their high photostability, high brightness, long luminescence decay time, tailorable and narrow emissions, and low toxicity. However, since this type of particles has a non-spherical shape and polarized emission, i.e. orientation-dependent luminescence intensity with respect to

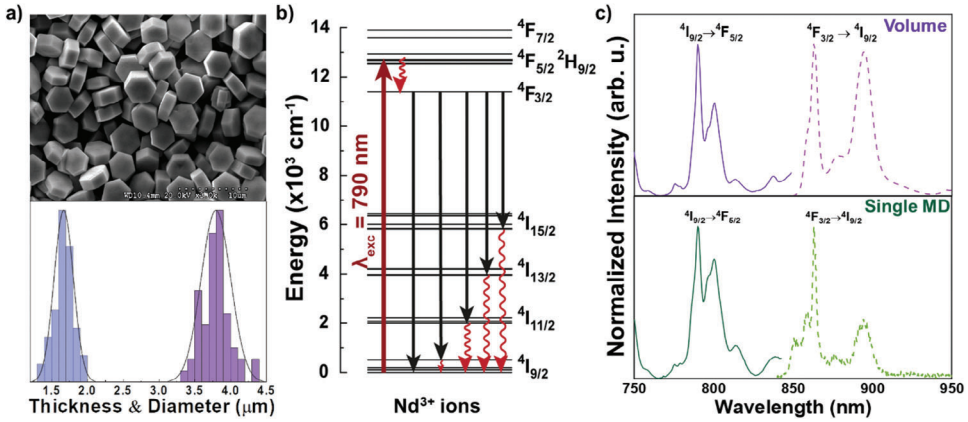

Figure 1. Characterization of the heating mMDs. a) SEM image of the disk-shaped $NaLuF_4$:Nd^{3+} microparticles and their size histogram in terms of thickness and diameter of the hexagonal phase. b) Energy levels diagram of the Nd^{3+} ions with the excitation transition at 790 nm, the main radiative transitions (dark arrows), and phonon relaxations (red curved arrows). c) Excitation spectra detected at 895 nm (violet and green solid curves), and emission spectra excited at 790 nm (pink and light green dashed curves), of a volume of microparticles and of a single trapped particle, normalized to the most intense transitions.

the polarization direction of excitation,[27] changes in orientation with respect to the optical axis of the laser beam while rotating can affect the amount of absorbed light and laser-induced polarizability, reducing the total heating. Therefore, this effect must be studied, as it can be significant for future applications of this type of combined microheater-rotors. The aim of this work is to explore the influence of orientation of a neodymium-doped β-$NaLuF_4$: 5% Nd^{3+} microdisk on local heating of a liquid medium at the microscale, under linearly and circularly polarized laser excitation.[9,28]

2. Results and Discussion

2.1. Spectroscopic Characterization

In this section, a thorough description of the particles used in this work and their luminescence processes are presented. Hexagonal disk-shaped $NaLuF_4$ microparticles doped with 5% Nd^{3+} ions were selected as local microheaters and spinners to study their heating performance at the microscale. They were synthesized by a hydrothermal process (see the Experimental Section) and present a mean diameter and thickness of 3.8 ± 0.2 μm and 1.7 ± 0.1 μm, respectively, as measured from scanning electron microscopy (SEM) images (**Figure 1a**). When one microdisk (MD) is excited with a 790 nm laser, the emission of the Nd^{3+} ions in the lattice is induced (see the energy levels diagram and transitions in Figure 1b). The excitation spectrum is depicted in Figure 1c for both a volume of microparticles and for a single MD optically trapped in water, obtained by monitoring the maximum emission wavelength (895 nm) while varying the excitation wavelength in the region from 750 to 840 nm. The excitation spectra show a band corresponding to transitions from the ground-state multiplet $^4I_9$ of the Nd^{3+} ions to their excited multiplet $^4F_{5/2}$, with the maximum excitation wavelength at 790 nm. On the other hand, the emission spectra present an structured emission band with two main peaks at 860 and 895 nm corresponding to the transitions of Nd^{3+} ions from the excited state $^4F_{3/2}$ to the ground-state multiplet $^4I_{9/2}$, split due to the effect of the crystal field. Therefore, after 790 nm excitation, the Nd^{3+} ions relax from the excited state $^4F_{5/2}$ to the $^4F_{3/2}$ state and NIR emissions are produced to populate the ^4I_J states, supported by multiphonon relaxation to the ground state $^4I_{9/2}$. Heat is generated with each nonradiative deexcitation, as the Nd^{3+} ions partially convert the laser excitation energy into heat by multiphonon relaxation but also due to cross relaxation to neighboring ions and energy migration to closely located non-radiative centers.[29] Consequently, it is expected that by exciting the Nd^{3+} ions at 790 nm, the maximum potential heat could be generated. For this reason, 790 nm was selected as the wavelength of the trapping and excitation laser in the experiments performed in this work.

2.2. Analysis of Rotational Dynamics of Single Microheaters

When excited with appropriate photoexcitation wavelengths, microparticles doped with a high content of Nd^{3+} ions are expected to generate heat by non-radiative deexcitations to the ground state of the Nd^{3+} ions and to transfer it to their surrounding medium.[9] To determine the dependence of the excitation wavelength and the influence of rotation on the amount of generated heat at the microscale, a single $NaLuF_4$:Nd^{3+} MD was spectroscopically characterized and optically trapped and rotated in water. To evaluate the temperature increment of the medium produced by the laser excitation of the MD, the thermal excitation spectrum was obtained: An aqueous colloidal dispersion of Nd^{3+}-doped MDs (microheaters) and commercial CdSe quantum dots (QDs) (luminescent nanothermometers) was placed in a homemade double-beam fluorescence and OT microscope (see the Experimental Setup section). The so-called thermal excitation spectrum was measured by trapping a MD with a Ti: Sapphire tunable laser in the 770–830 nm wavelengths range, while simultaneously exciting the luminescent nanothermometers with a second laser beam at 488 nm to measure the local temperature increment in the surrounding water. In other words, a single $NaLuF_4$:Nd^{3+} MD stayed under illumination by the tunable trapping laser during the complete duration of the experiment, while

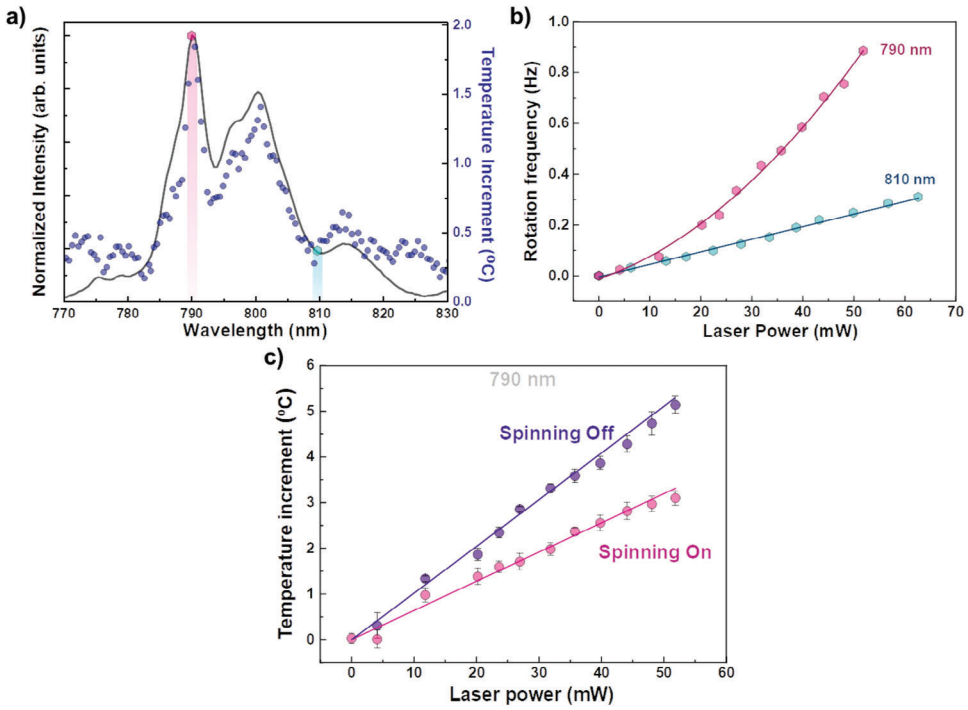

Figure 2. Characterization of the heating effect. a) Normalized excitation spectrum (black curve) of a single trapped microdisk, detected at 895 nm, along with its thermal spectrum (blue points), that is, temperature changes at different excitation wavelengths obtained by analyzing the nanothermometer emission recorded in the surroundings of a trapped MD by a 40 mW laser. b) Rotation frequency as a function of laser power for two different trapping-excitation laser wavelengths, 790 and 810 nm, corresponding to high and low laser absorption, respectively, as measured in (a). c) Temperature increment in the surrounding medium of a single MD optically trapped with a 790 nm linearly polarized laser beam (MD static in the trap, purple data) and circularly polarized beam (MD spinning, pink data) as a function of the applied laser power.

the local temperature in the surrounding region was monitored by the emission of the nanothermometers. It is important to clarify that the 488 nm laser was aligned and focused on the same position of the trapping spot laser and the objective lenses used to focus each laser were specially selected to provide comparable excitation areas (spot sizes $A_{trap} \sim 2.2\ \mu m^2$ and $A_{488} \sim 1.7\ \mu m^2$, as calculated in Section 2 of the Supporting Information). The 488 nm photoexcitation did not excite the Nd^{3+} ions in the trapped MD, only the luminescence of the nanothermometers was observed. Moreover, in the 770–830 nm range of wavelengths and the low power used (40 mW), the absorption of water is negligible. In addition, for the nanothermometer's concentration and 488 nm laser power used in this work, no thermal loading of the mixed solution was produced due to the light absorption of the nanothermometers (their luminescence band only shifted in the presence of a trapped heating MD). Therefore, the light-induced heating should be only related to the MD absorption, which varies with the excitation wavelength and orientation. This is corroborated in **Figure** 2a by the overlap between the thermal excitation spectrum (blue circles) and the excitation spectrum of a single microdisk (black line). Indeed, the thermal excitation spectrum reproduces the spectral shape of the excitation spectrum of a neodymium-doped MD. Therefore, the optical absorption of the MD governs the light-to-heat conversion. During the emission process, the MD delivered heat to its surrounding medium with a maximum temperature increment of ≈2 °C produced by photoexcitation at 790 nm.

Once the heating capability of a single trapped MD is demonstrated, it is crucial to know how the luminescence properties and orientation of the rotating MD affect the local temperature of its surrounding medium before further developing an actual application. When illumination is performed at a low absorption wavelength (i.e., 810 nm), the rotation frequency increases linearly with the applied power following Equation (4), see Figure 2b, as heating is negligible at this laser wavelength. However, for 790 nm photoexcitation, the rotation frequency of the MD increases faster than for the non-absorbed wavelength of excitation, following a supra-linear trend that evidences the temperature increase of the surrounding medium. This response is related to the induced heating at the Nd-doped MD absorbing wavelength, which leads to a decrease of the medium viscosity, resulting in higher rotation speeds. However, at low laser powers the MD behaves linearly and, as there is no heating, the influence of the trapping laser wavelength on the angular velocity is negligible and rotation can be considered only due to the particle birefringence. This is corroborated in Section 3 of the Supporting Information, where the normalized rotation rate of the particle at the low laser power regime is represented in Figure S3 (Supporting Information).

The temperature increase of the surrounding medium for the high-absorbed 790 nm photoexcitation was experimentally determined following the same process previously described (i.e., analyzing the red shift of the nanothermometers emission suspended in the surroundings of the MD). As shown in Figure 2c,

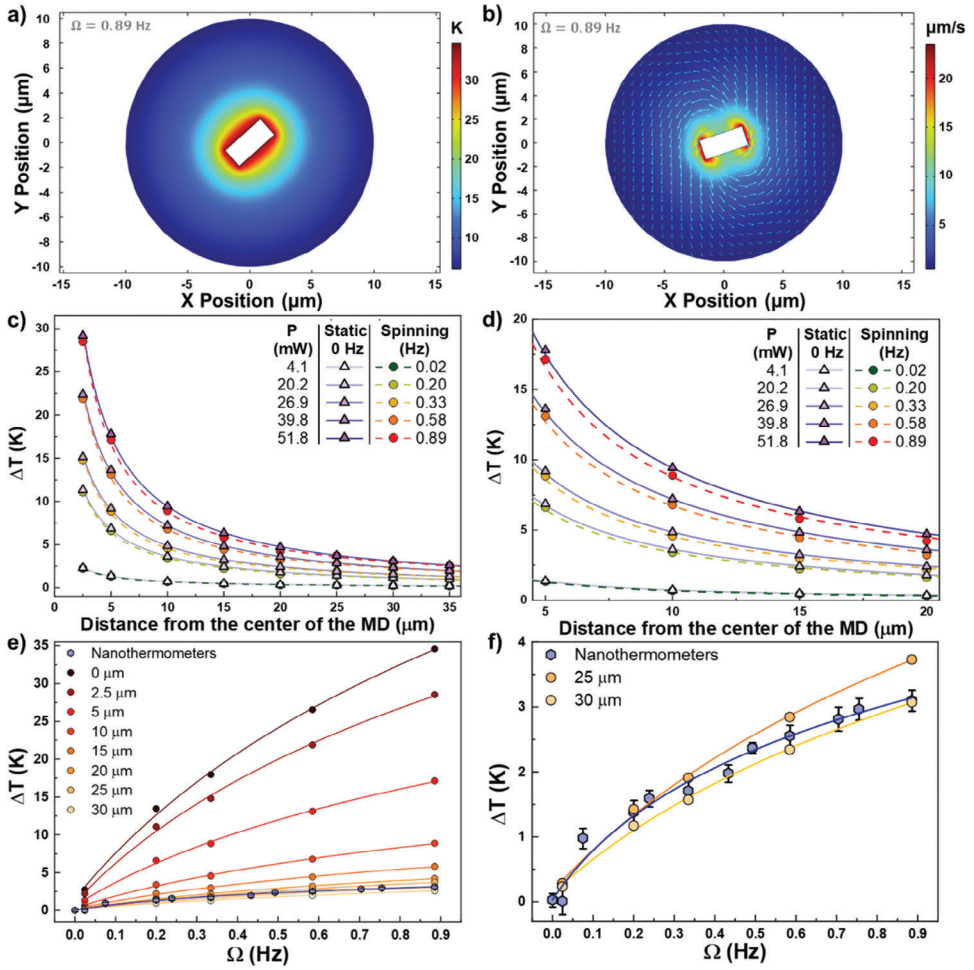

Figure 3. Simulation results and comparison with experiments. a) Simulation of the water temperature increase in a horizontal plane of a microdisk (white rectangle) rotating at 0.89 Hz after 1.15 s. b) Simulation of the velocity vector field in the same plane and conditions as (a). c) Estimated temperature increments for different laser powers of a static and a spinning microdisk, considering different radii of analysis from the center of the microdisk. d) Zoomed version of (c) to see the deviation between the static and spinning particle results. e) Temperature increment as a function of the angular velocity for the experimental measurements and simulations considering several areas of radius. f) Zoom of (e), only considering the experimental measurements and two simulations considering regions of 15 and 20 μm of radius.

in the case of linearly polarized photoexcitation, the temperature in the surroundings of the trapped static MD (i.e. its optical axis aligned with the electric field vector of the laser trapping beam) increases linearly with the laser power, at a rate of $c = 0.102 \pm 0.002$ °C mW^{-1}, which is of the same order of magnitude as that reported for colloidal dispersions of Nd-doped nanoparticles and for similar $NaYF_4$: Er^{3+}, Nd^{3+} microdisks.[25,26,28,30] It suggests a reasonable light-to-heat conversion efficiency of the studied particles, which is then transferred to the surrounding medium. Compared to the static conditions, temperature increases at a lower rate (0.063 ± 0.001 °C mW^{-1}) when the trapped MD is spinning. This result suggests that rotation affects the process involved in heat generation and heat transfer to its surrounding medium. Interestingly, since the heating mechanism is based on the non-radiative de-excitations produced in the luminescence process of the Nd^{3+} ions, and the luminescence intensity is orientation-dependent with respect to the polarization angle of the photoexcitation, the results reveal that the heating process will also depend on the polarized absorption and emission of the $NaLuF_4$ anisotropic MD.

A simulation with the COMSOL Multiphysics finite-element analysis platform was carried out to evaluate this proposed relationship between orientation and heating of lanthanide-doped MDs. The simulation is detailed in the Simulation section of Experimental Section. The surface temperature of the MD was calculated from the supra-linear trend of the experimental angular velocity following the fitting curve $\Omega(P, T)$ mentioned previously (see Supporting Information for the detailed explanation). **Figure 3a** shows the simulated temperature distribution in the water surrounding the spinning MD (white rectangular section) for a horizontal cut when rotating at 0.89 Hz. Similar results were obtained at moderately higher rotation rates (data not shown). The corresponding velocity vector field is also shown in Figure 3b. However, depending on the applied laser power, P, the rotation frequency, and the generated heat will vary. For this reason, the

simulation was performed for different surface temperatures (calculated from Figure 2b, see Supporting Information), corresponding to the different laser powers applied, with and without the MD spinning. As shown in Figure 3c and its zoom Figure 3d, heat diffuses with respect to the distance from the particle and its variation from the static to the spinning particle is small. Thus, for this range of velocities, the decrease in transferred heat cannot be associated with heating dissipation due to the stirring of the liquid medium. Alternatively, the photothermal effect observed in this experiment must be associated with the laser-MD axis misalignment while rotating, which will affect the absorption of light by the trapped MD and thus be related to the polarized absorption process. Also, an unequal temperature distribution around the spinning MD could occur and affect the overall heating measured in the medium. Furthermore, Figure 3e shows the temperature increase as a function of the angular velocity for different distances from the heating and spinning MD. The experimental data obtained from the nanothermometers emission (violet hexagons and line) are proximal to the 25 and 30 μm radii, as can be appreciated in the amplified Figure 3f. The experimental radius of detection comes from the 488 nm laser spot focused by a 0.6 NA objective lens, which excited the nanothermometers suspended in the water surrounding the microdisk. Theoretically, the generated spot of ω_{488} ~2 μm is comparable to the thickness of the particle (1.7 ± 0.1 μm), as calculated in the Supporting Information. However, the profile of the 488 nm laser beam can be reasonably extended to the 30 μm obtained from simulations, as previous results showed a 50 μm profile for a heating 980 nm beam measured with QDs in the same experimental setup.[31] In addition, the 488 nm laser could not only excite the nanothermometers in the horizontal plane, but that suspended slightly out-of-focus in the three-dimensions surrounding the particle. For this reason, the experimentally obtained heating of the liquid medium at the microscale is reduced in comparison to the internal heating of the microdisk calculated from the supra-linear angular velocity, as expected. This should be carefully noted to avoid overestimating heating by the rotation dynamics analysis of luminescent birefringent particles.

As a future perspective, the use of confocal detection configuration for the emission thermometry would allow an increase in the spatial selectivity, reducing the discrepancy. This could be a promising way to experimentally characterize the heating of the medium in 3D.

3. Conclusion

In this work, a hexagonal disk-shaped $NaLuF_4$: Nd^{3+} microheater was optically trapped and rotated in water to study its local heat generation and heat transfer to a liquid medium at the microscale. The influence of the laser wavelength, power, and polarization on the thermal effect was studied. The measurement of temperature was achieved by spectral luminescence thermometry, using nanometric CdSe QDs dispersed in the medium as thermal probes. When a single Nd-doped microdisk was remotely trapped with 790 nm photoexcitation, the temperature of the surrounding water increased linearly with the applied laser power due to the Nd^{3+} absorption, which is maximum at this wavelength. It was found that the maximum heating was achieved when the particle was static in the trap, while the magnitude of transferred heat was smaller for the rotating particle. Surprisingly, this result was not associated with the stirring of the medium and fluid displacement, as simulations corroborated. Alternatively, the difference in temperature increase with and without rotation can be explained by the orientation-dependent absorption of the $NaLuF_4$: Nd^{3+}, that is, the angle between the polarization of the excitation light and the optical axis of the hexagonal $NaLuF_4$: Nd^{3+} affect the amount of absorbed light and laser-induced emission, reducing the total heating. These results emphasize the importance of polarization for this type of luminescent uniaxial birefringent crystalline particles for thermal and microfluidic applications. When working with these lanthanide-doped particles in the micro or nanoscale, their orientation with respect to the laser source can be critical, and in the case of spinning particles, the predicted temperature change has to be cautiously estimated. Therefore, local thermal and viscosity changes in a liquid can be calculated from the rotation dynamics analysis, but it needs to be carefully treated to obtain the real particle-liquid heat transfer in the surrounding volume.

4. Experimental Section

Sample Preparation: The $NaLuF_4$:Nd^{3+} microparticles were synthesized by the hydrothermal method. Aqueous solution of sodium citrate and $Lu(NO_3)_3$ was mixed under vigorous stirring to form a milky suspension, into which an aqueous solution of NaF was added to obtain a transparent colloidal. The resulted colloidal was then heated to 220 °C for 12 h.

Experimental Setup: In this section, a thorough description of the experimental set-up is presented.

An aqueous colloidal dispersion of both MDs and nanothermometers, stirred to avoid clusters, was prepared in a 120-μm height microchamber, which was then placed in a homemade double beam fluorescence and optical trapping microscope (see **Figure 4a** for a schematic representation of the setup used in this work). The upper part of the experimental setup allowed the OT of a single MD and its rotation (using circularly polarized light obtained by a quarter-wave plate placed after the linearly polarized Gaussian beam of the laser). A complementary metal-oxide-semiconductor (CMOS) camera coupled to the set-up was used to visualize the motion of the MD. The $NaLuF_4$:Nd^{3+} MDs are positive uniaxial birefringent crystals whose optical axis is perpendicular to the two facets of the crystal, so a single trapped MD orientates in its vertical position with its hexagonal facets parallel to the propagation direction of the optical trap. Due to their birefringent nature, when a circularly polarized beam traps the MD, angular momentum transfer light-to-microdisk occurs, which induces an optical torque and the rotation of the MD. Thus, the particle rotates with an angular velocity following Equation (4), as it can be monitored in real time with the camera. Figure 4b shows the rotation of the MD around its longitudinal axis in the form of two chronological frames. Further, the lower section of the setup allowed the analysis of the rotation dynamics of the trapped particle and the thermal sensing. The angular velocity of the MD was obtained by tracking the displacements of the optically trapped MD with a quadrant photodetector (QPD), which detected the light scattered by the rotating particle using back focal plane interferometry. A representative spectrum of the angular frequency is presented in Figure 4c. To assess the local heating of the Nd-doped MD as a result of their laser excitation and the heat transfer to their surrounding medium, QDs were used as thermal local nanoprobes dispersed in the liquid.[6b,10] Due to their reliability and the characteristic temperature-induced red shift of their luminescence band, QDs are commonly applied for thermal sensing. Commercial CdSe-QDs were used in this work (Qdot 655 ITK, Invitrogen), of mean size 12 ± 1 nm as measured from transmission electron microscopy images (see Supporting Information). Local

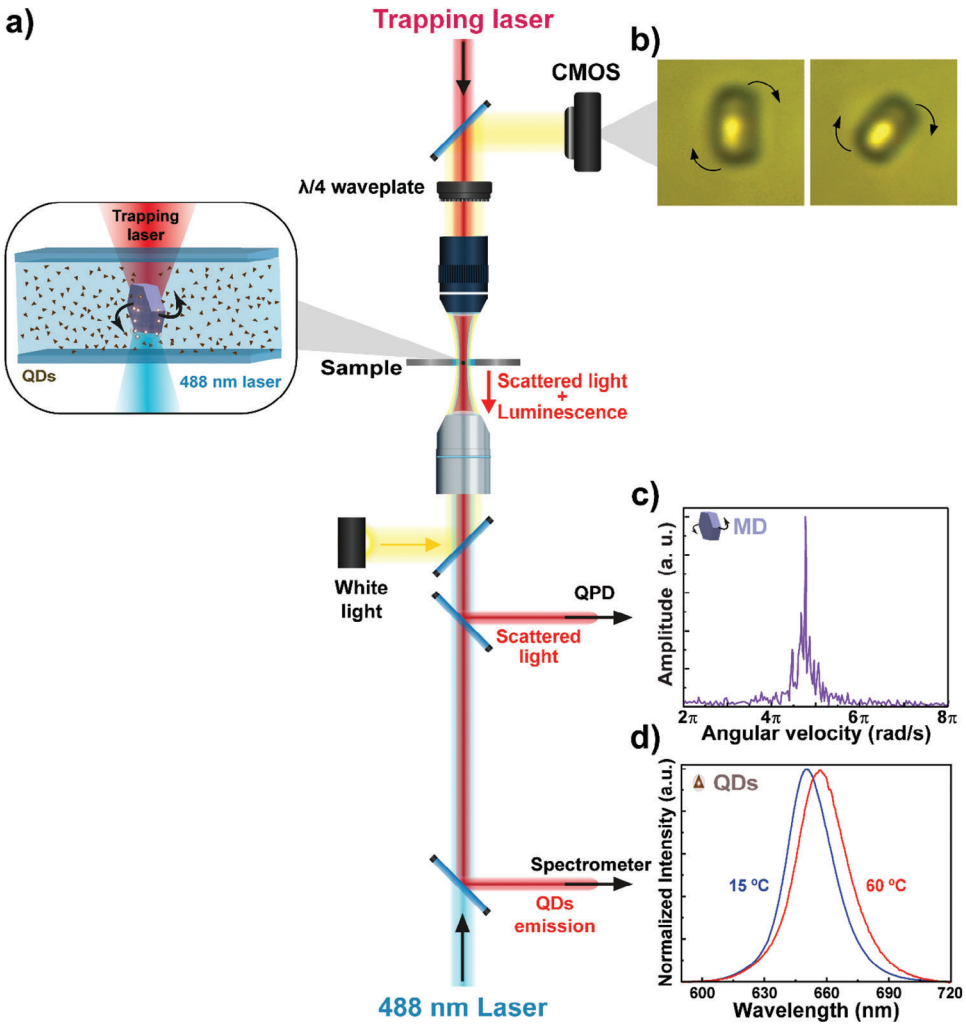

Figure 4. Experimental setup and measurement strategy. a) Schematic representation of the experimental setup for OT. Inset: A zoomed image of the sample, consisting of a single microdisk trapped in a water dispersion of CdSe quantum dots (QDs). The microdisk is optically manipulated with the trapping laser, and its visualization was performed with a CMOS camera, as seen in the image sequence in (b). The position of the microdisk and the rotational frequency are measured with a QPD. c) Representative rotational frequency spectrum. d) The temperature-dependent luminescence of the CdSe QDs is excited with a 488 nm diode laser and detected using an Ocean Optics spectrometer coupled to the setup.

thermal sensing was performed by analyzing the fluorescence of the QDs located in the surroundings of the trapped MD. The excitation source was a 488 nm diode laser focused and aligned on the trapped particle so the calculated temperature from the QDs emission corresponded to that of the surrounding medium. The luminescence was recorded with a fiber-coupled Ocean Optics QE65000 High-Sensitivity Fiber Optic Spectrometer, with a wavelength range of detection of 400–700 nm and a spectral resolution of 0.4 nm. Two emission spectra measured in the experimental setup at low and high temperature are displayed in Figure 4d. The central wavelength of the QDs emission peak shifts linearly toward longer wavelengths with increasing temperature at a rate of 0.131 ± 0.001 nm K^{-1} (see Figure S1, Supporting Information), which can be used to measure temperature changes.

Simulations: Heat generation and transport were simulated using the COMSOL Multiphysics finite-elements analysis platform. To this end, a 50 µm-radius and 100 µm-height cylinder was considered to model the water domain and a 3.8 µm of diameter and 1.7 µm-height small cylinder was modeled to resemble the disk-shaped microparticle. The axis of the latter cylinder is perpendicular to that of the water domain.

To perform a simulation that could be compared with experiments, a model was configured considering the trapped particle with a rotation produced by the inherent characteristics of its material. This model includes the Heat Transfer in Fluids and Solids, the Laminar Flow physics interfaces as well as the Nonisothermal Flow Multiphysics coupling. Additionally, the Moving Mesh physics was introduced to consider the rotation of the particle in the model.

Due to the unknown value of the absorption cross-section of the $NaLuF_4$:Nd^{3+} microparticle, it was necessary to estimate the temperature on the surface of the particle. This value was introduced in the simulation as a thermal boundary condition. Moreover, a fixed temperature condition was considered at the domain's boundaries. Regarding the laminar flow, it was not necessary to introduce more boundary conditions apart from the default ones included by the program.

After the mesh was adequately configured, a time-dependent study was introduced. It is important to note that the time steps of the studies vary with respect to the different values of the rotation speed. To calculate the model for all the laser power values, a comprehensive parametric sweep was defined.

Supporting Information

Supporting Information is available from the Wiley Online Library or from the author.

Acknowledgements

This work was financially supported by projects CNS2022-135495, PID2023-151078OB-I00 and TED2021-129937B-I00 funded by MCIN/AEI/10.13039/501100011033 and by the "European Union NextGenerationEU/PRTR". E.O.R. gratefully acknowledges the financial support provided by the Spanish Ministerio de Universidades, through the FPU program (FPU19/04803). R.A.R. and C.D.G.G. acknowledge financial support provided by Consejería de Universidad, Investigación e Innovación de la Junta de Andalucía and by FEDER "Una manera de hacer Europa" (P18-FR-3583).

Conflict of Interest

The authors declare no conflict of interest.

Data Availability Statement

The data that support the findings of this study are available from the corresponding author upon reasonable request.

Keywords

heat transfer, nanothermometers, neodymium, optical trapping, polarized luminescence, rare-earth, remote sensing

Received: September 25, 2023
Revised: March 3, 2024
Published online:

[1] a) G. Maltezos, A. Gomez, J. Zhong, F. A. Gomez, A. Scherer, *Appl. Phys. Lett.* **2008**, *93*, 243901; b) G. Maltezos, M. Johnston, K. Taganov, C. Srichantaratsamee, J. Gorman, D. Baltimore, W. Chantratita, A. Scherer, *Appl. Phys. Lett.* **2010**, *97*, 264101.

[2] a) P. Paik, V. K. Pamula, K. Chakrabarty, *The Ninth Intersociety Conf. on Thermal and Thermomechanical Phenomena In Electronic Systems*, IEEE, **2004**, 649–654; b) P. Laval, N. Lisai, J.-B. Salmon, M. Joanicot, *Lab on a Chip.* **2007**, *7*, 829.

[3] a) J. Lu, X.-J. Wang, C.-B. Ching, *Progr. Cryst. Growth Character. Mater.* **2002**, *45*, 201; b) M. M. Islam, S. Nakamura, K. Noguchi, M. Yohda, S.-i. Kidokoro, Y. Kuroda, *Cryst. Growth Design.* **2015**, *15*, 2703.

[4] S.-J. Kim, F. Wang, M. A. Burns, K. Kurabayashi, *Analyt. Chem.* **2009**, *81*, 4510.

[5] a) D. Jaque, L. M. Maestro, B. Del Rosal, P. Haro-Gonzalez, A. Benayas, J. Plaza, E. M. Rodriguez, J. G. Sole, *Nanoscale.* **2014**, *6*, 9494; b) M. Quintanilla, I. García, I. de Lázaro, R. García-Alvarez, M. Henriksen-Lacey, S. Vranic, K. Kostarelos, L. M. Liz-Marzán, *Theranostics.* **2019**, *9*, 7298.

[6] a) M. Quintanilla, L. M. Liz-Marzán, *Nano Today.* **2018**, *19*, 126; b) C. D. S. Brites, A. Millán, L. D. Carlos, *Handbook on the Physics and Chemistry of Rare Earths*, Elsevier, **2016**, *49*, 339–427; c) G. López-Peña, K. Hamraoui, K. Horchani-Naifer, C. Gerke, D. H. Ortgies, E. Martín Rodríguez, G. Chen, D. Jaque, J. Rubio Retama, *Phys. B: Condens. Matter.* **2022**, *631*, 413652.

[7] a) E. Hemmer, P. Acosta-Mora, J. Méndez-Ramos, S. Fischer, *J. Mater. Chem. B.* **2017**, *5*, 4365; b) E. Carrasco, B. del Rosal, F. Sanz-Rodríguez, Á. J. Fuente, P. H. Gonzalez, U. Rocha, K. U. Kumar, C. Jacinto, J. G. Solé, D. Jaque, *Adv. Funct. Mater.* **2015**, *25*, 615; c) A. Bednarkiewicz, D. Wawrzynczyk, M. Nyk, W. Strek, *Appl. Phys. B.* **2011**, *103*, 847.

[8] a) Y. Shen, H. D. A. Santos, E. C. Ximendes, J. Lifante, A. Sanz-Portilla, L. Monge, N. Fernández, I. Chaves-Coira, C. Jacinto, C. D. S. Brites, L. D. Carlos, A. Benayas, M. C. Iglesias-de la Cruz, D. Jaque, *Adv. Funct. Mater.* **2020**, *30*, 2002730; b) S. T. Dibaba, Y. Xie, W. Xi, A. Bednarkiewicz, W. Ren, L. Sun, *J. Rare Earths.* **2022**, *40*, 862.

[9] B. del Rosal, U. Rocha, E. C. Ximendes, E. Martín Rodríguez, D. Jaque, J. G. Solé, *Opt. Mater.* **2017**, *63*, 185.

[10] D. Jaque, F. Vetrone, *Nanoscale.* **2012**, *4*, 4301.

[11] a) B. del Rosal, D. H. Ortgies, *21st Century Nanoscience–A Handbook*, CRC Press, **2020**, 24; b) M. Quintanilla, M. Henriksen-Lacey, C. Renero-Lecuna, L. M. Liz-Marzán, *Chem. Soc. Rev.* **2022**, *51*, 4223.

[12] a) A. Ashkin, *Phys. Rev. Lett.* **1970**, *24*, 156; b) A. Ashkin, *J. Opt. Soc. Am. A.* **1985**, *2*, P50; c) A. Ashkin, J. M. Dziedzic, T. Yamane, *Nature.* **1987**, *330*, 769.

[13] a) P. Rodriguez-Sevilla, L. Labrador-Paez, D. Jaque, P. Haro-Gonzalez, *J. Mater. Chem. B.* **2017**, *5*, 9085; b) P. M. Bendix, L. Jauffred, K. Norregaard, L. B. Oddershede, *IEEE J. Sel. Top. Quantum Electron.* **2014**, *20*, 3.

[14] U. Rocha, K. Upendra Kumar, C. Jacinto, J. Ramiro, A. J. Caamaño, J. García Solé, D. Jaque, *Appl. Phys. Lett.* **2014**, *104*, 053703.

[15] a) P. Galajda, P. Ormos, *Appl. Phys. Lett.* **2001**, *78*, 249; b) Z.-P. Luo, Y.-L. Sun, K.-N. An, *Appl. Phys. Lett.* **2000**, *76*, 1972; c) N. B. Simpson, K. Dholakia, L. Allen, M. J. Padgett, *Opt Lett.* **1997**, *22*, 52.

[16] a) K. Miyakawa, H. Adachi, Y. Inoue, *Appl. Phys. Lett.* **2004**, *84*, 5440; b) D. Haefner, S. Sukhov, A. Dogariu, *Phys. Rev. Lett.* **2009**, *103*, 173602; c) D. Gao, W. Ding, M. Nieto-Vesperinas, X. Ding, M. Rahman, T. Zhang, C. Lim, C.-W. Qiu, *Light: Sci. Amp; Appl.* **2017**, *6*, 17039.

[17] P. Rodriguez-Sevilla, L. Labrador-Paez, D. Wawrzynczyk, M. Nyk, M. Samoc, A. K. Kar, M. D. Mackenzie, L. Paterson, D. Jaque, P. Haro-Gonzalez, *Nanoscale.* **2016**, *8*, 300.

[18] P. Rodriguez-Sevilla, T. Lee, L. Liang, P. Haro-González, G. Lifante, X. Liu, D. Jaque, *Adv. Opt. Mater.* **2018**, *6*, 1800161.

[19] P. Rodríguez-Sevilla, Y. Zhang, P. Haro-González, F. Sanz-Rodríguez, F. Jaque, J. G. Solé, X. Liu, D. Jaque, *Adv. Mater.* **2016**, *28*, 2421.

[20] a) E. Ortiz-Rivero, K. Prorok, I. R. Martín, R. Lisiecki, P. Haro-González, A. Bednarkiewicz, D. Jaque, *Small.* **2021**, *17*, 2103122; b) A. K. Vuppu, A. A. Garcia, S. K. Saha, P. E. Phelan, M. A. Hayes, R. Calhoun, *Lab on a Chip.* **2004**, *4*, 201; c) C. Zhang, K. Khoshmanesh, A. Mitchell, K. Kalantar-Zadeh, *Analyt. Bioanalyt. Chem.* **2010**, *396*, 401.

[21] a) H. Chen, Q. Zhao, X. Du, *Micromachines.* **2018**, *9*, 41; b) H. Rubinsztein-Dunlop, T. Asavei, A. B. Stilgoe, V. L. Loke, R. Vogel, T. A. Nieminen, N. R. Heckenberg, *Design of Optically Driven Microrotors*, CRC Press, Boca Raton, FL **2012**, pp 277–306; c) S. Maruo, *Microfluidic Technologies for Miniaturized Analysis Systems*, (Eds., S. Hardt, F. Schönfeld), Springer, Berlin, Germany **2007**, pp 275–314.

[22] S. J. Parkin, G. Knöner, T. A. Nieminen, N. R. Heckenberg, H. Rubinsztein-Dunlop, *Phys. Rev. E.* **2007**, *76*, 041507.

[23] X. Zou, Q. Zheng, D. Wu, H. Lei, *Adv. Funct. Mater.* **2020**, *30*, 2002081.

[24] C. J. Bustamante, Y. R. Chemla, S. Liu, M. D. Wang, *Nat. Rev. Methods Prim.* **2021**, *1*, 25.

[25] a) A. I. Bishop, T. A. Nieminen, N. R. Heckenberg, H. Rubinsztein-Dunlop, *Phys. Rev. Lett.* **2004**, *92*, 19; b) M. E. J. Friese, T. A. Nieminen, N. R. Heckenberg, H. Rubinsztein-Dunlop, *Nature.* **1998**, *394*, 348.

[26] L. Shao, Z.-J. Yang, D. Andrén, P. Johansson, M. Käll, *ACS Nano.* **2015**, *9*, 12542.

[27] P. Chen, M. Song, E. Wu, B. Wu, J. Zhou, H. Zeng, X. Liu, J. Qiu, *Nanoscale.* **2015**, *7*, 6462.

[28] U. Rocha, K. U. Kumar, C. Jacinto, J. Ramiro, A. J. Caamaño, J. G. Solé, D. Jaque, *Appl. Phys. Lett.* **2014**, *104*, 053703.
[29] E. H. Otal, F. A. Iñón, F. J. Andrade, *Appl. Spectrosc.* **2003**, *57*, 661.
[30] a) V. Miralles, A. Huerre, F. Malloggi, M.-C. Jullien, *Diagnostics.* **2013**, *3*, 33; b) B. del Rosal, A. Pérez-Delgado, E. Carrasco, D. J. Jovanović, M. D. Dramićanin, G. Dražić, Á. J. Fuente, F. Sanz-Rodriguez, D. Jaque, *Adv. Opt. Mater.* **2016**, *4*, 782.
[31] P. Haro-González, B. del Rosal, L. M. Maestro, E. Martín Rodríguez, R. Naccache, J. A. Capobianco, K. Dholakia, J. G. Solé, D. Jaque, *Nanoscale.* **2013**, *5*, 12192.